JCI insight

RESEARCH ARTICLE

High pathogen burden in childhood promotes the development of unconventional innate-like CD8+ T cells

Yves T. Falanga,[1,2] Michela Frascoli,[2] Yasin Kaymaz,[3] Catherine Forconi,[2] John Michael Ong'echa,[4] Jeffrey A. Bailey,[3,5] Leslie J. Berg,[1] and Ann M. Moormann[2]

[1]Department of Pathology, [2]Program in Molecular Medicine, and [3] Program in Bioinformatics and Integrative Biology, University of Massachusetts Medical School, Worcester, Massachusetts, USA. [4]Center for Global Health Research, Kenya Medical Research Institute, Kisumu, Kenya. [5]Division of Transfusion Medicine, Department of Medicine, University of Massachusetts Medical School, Worcester, Massachusetts, USA.

Cellular and humoral constituents of the immune system differ significantly between children and adults, yet very little is known about the impact of early-life pathogen exposure on this immunologic transition. We examined CD4+ and CD8+ T cell subsets defined by CCR7 and CD45RA expression in two longitudinal pediatric cohorts experiencing divergent levels of pathogen burden. Using multiparameter flow cytometry, along with serological, cytokine, and transcriptomic data, we show that cumulative pathogen burden promotes the development of atypical $CD8^{dim}$ T cells with an innate-like profile (Granzyme B^{hi}, $IFN\gamma^{low}$, $TNF\alpha^{low}$, $PLFZ^{hi}$, $ID2^{hi}$, $IKZF2^{hi}$) in contrast to age-matched children residing in a low pathogen–exposure area who display a more conventional $CD8^{bright}$ profile ($IFN\gamma^{+}$, $TNF\alpha^{+}$, $CCL4^{+}$). Furthermore, these unconventional T cells had stunted proliferation, distinct transcriptional programs, and impaired T cell receptor signaling and were enriched in hallmark TNFα, NF-κB, and IL-6 gene signaling pathways, reminiscent of NK cells and type-1 innate lymphoid cells. Our findings suggest that these unconventional $CD8^{dim}$ T cells arise in a very particular immunological context and may provide a deeper understanding of the heterogeneity in human immune responses.

Introduction

The adaptive immune system has evolved to mount effective and specific immune responses to pathogenic infections that provide protective memory against future exposures (1–4). Although animal models have been essential to decipher key immunological processes, they are limited in their ability to recapitulate the substantial heterogeneity within and between humans that contributes to the balance between protection and pathology (5, 6). Chronic or repeated infections pose a challenge to the host. An overexuberant response may lead to immune pathology, while a weak response may lead to pathogens overwhelming the host. Overall, there are substantial gaps in our understanding of how pathogens, particularly chronic or repeated infections, interplay and affect the development of the human immune system during infancy and early childhood (5, 6). Also, studies of the immune system in children are challenging due to inherent difficulties in collecting samples and the logical limitations imposed on quantity and accessible immune compartments.

Plasmodium falciparum (Pf). malaria infections of children residing in endemic areas initially present as acute, symptomatic infections that evolve into chronic, asymptomatic infections after repeated, high-dose exposures (7, 8). The immunologic transition that results in premunition, also referred to as clinical immunity or immune tolerance, is not fully understood and becomes challenging to deconvolute from immunologic maturation that naturally occurs as children age. Seminal studies have elegantly demonstrated the association of clinical immunity to malaria with a decreased number and function of $V\gamma2^{+}V\delta2^{+}$ cells, a subset of γδ T lymphocytes that does not require antigen processing to induce T cell receptor–mediated (TCR-mediated) cytolytic death of infected red blood cells via granulysin (9–13). These findings support the premise that persistent malaria infection induces immunological adaptation in humans, favoring a less inflammatory environment. Although numerous studies have shown that children's and adults' immune systems differ in multiple aspects (5, 6, 14, 15), very little is known about how pathogen exposure affects the transition of naive $CD8^{+}$ T cells to effector and effector memory cells in humans.

Conflict of interest: The authors have declared that no conflict of interest exists.

Submitted: March 6, 2017
Accepted: June 20, 2017
Published: August 3, 2017

Reference information:
JCI Insight. 2017;2(15):e93814.
https://doi.org/10.1172/jci.insight.93814.

Chronic parasitic and viral infections have been shown to cause T cell exhaustion, a phenomenon characterized by a hierarchical degradation of pathogen-specific T lymphocytes that lose their ability to mount cytolytic and other effector functions upon TCR stimulation (16–18). Furthermore, mechanisms by which chronically infected individuals with potent and nonexhausted T cells are able to sustain elevated pathogen burden without displaying life-threatening clinical signs remain poorly understood. To better understand the natural progression of T cells from naive-like to effector-memory subsets and changes in functionality, we prospectively compared two cohorts of age-matched children residing in areas with divergent pathogen burden (notably Pf and Schistosoma mansoni [Sm]) in western Kenya (19–21). We hypothesized that elevated cumulative pathogen burden would lead to T cell exhaustion and a significantly diminished capacity to respond to cognate antigen. Interestingly, and to our surprise, we found that over time, cumulative malaria and other infections promoted the development of unconventional innate-like $CD8^+$ T cells (Granzyme B^{hi}, $IFN\gamma^{low}$, $TNF\alpha^{low}$, $PLFZ^{hi}$, $ID2^{hi}$, $IKZF2^{hi}$) reminiscent of NK cells and type-1 innate lymphoid cells (ILC1) (22–24).

Results

Children living in areas of high pathogen burden have elevated proportions of $CD3^+CD8^{dim}$ T cells. The study's primary goal was to understand the impact of holoendemic Pf exposure on the development and function of $CD4^+$ and $CD8^+$ T cells. However, the high malaria transmission region (Kisumu, Kenya) from which study participants were enrolled also experience higher exposure to other chronic infections such as Sm and Epstein-Barr virus (EBV) compared with the low malaria exposure region (Nandi, Kenya) (19–21, 25). Nandi and Kisumu children are both infected with EBV early in life, and even though EBV is a persistent gammaherpesvirus, Nandi children have lower viral loads during childhood (26). Therefore, the two cohorts were defined as high pathogen burden and low pathogen burden cumulative childhood exposures for Kisumu and Nandi, respectively (Figure 1A and Supplemental Figure 1; supplemental material available online with this article; https://doi.org/10.1172/jci.insight.93814DS1) (19, 25, 26).

In order to evaluate the impact of chronic pathogen exposure on the development and effector function of $CD8^+$ T cells as children age, we analyzed peripheral blood mononuclear cells (PBMCs) from the same children at approximately 2.5 years (toddlers) and again at 6.5 years of age (school-age). In order to minimize investigator-based bias frequently encountered in flow cytometry gating strategies, in favor of a data-driven approach, we analyzed flow cytometry data with ACCENSE (27) and PhenoGraph (28), two platforms performing dimensionality reduction via t-distributed stochastic neighbor embedding (t-SNE) (29, 30) and partitioning of high-dimensional single cell data into subpopulations (Figure 1, B and C). Using this unsupervised approach on each study participant's PBMCs revealed partitioning of $CD3^+CD8^+$ T cells into two groups based on surface expression of the CD8 molecule: $CD8^{bright}$ and $CD8^{dim}$ T cells (Figure 1B). Megacluster analysis of unstimulated individual samples on a population level using PhenoGraph (28) showed that PBMCs from Kisumu (high pathogen burden) school-age children were significantly enriched in $CD8^{dim}$ clusters (Figure 1C) compared with their age-matched counterparts from Nandi (low pathogen burden).

While both groups displayed comparable proportions of $CD8^{dim}$ T cells during toddlerhood (median 11.2% and 14.6%), we observed that over time, children from Kisumu had significantly higher proportions of $CD8^{dim}$ T cells (46.1%) when they reached school age compared with their age-matched counterparts from Nandi (6.7%) (Figure 2, A and B). There was no significant difference in $CD8^{dim}$ absolute cells count between Nandi and Kisumu school-age study participants (Figure 2B). Both $CD8^{bright}$ and $CD8^{dim}$ T cells displayed comparable survival and viability as previously reported (31–34). While $CD8^+$ T cell subsets (defined by CCR7 and CD45RA staining) from Nandi and Kisumu children showed no substantial differences in proportions, the majority (~60%) of $CD8^{bright}$ T cells had a naive phenotype, while over 80% of the $CD8^{dim}$ cells were effector memory T cells (T_{EM}) and effector memory RA T cells (T_{EMRA}) (Figure 2, C and D), as observed previously (31, 32). Interestingly, there were no significant differences in the proportions of $CD4^+$ T cells functional subsets within our study populations as the children aged (Figure 2D). To our knowledge, our findings provide longitudinal epidemiological and immunological support for the uncharacteristic increase in $CD8^{dim}$ T cell proportions in the context of chronic parasitic infections in humans.

Elevated parasite-specific antibody titers are associated with increased proportions of $CD8^{dim}$ T cells. Although our cohorts were initially defined based on malaria transmission intensity, these children also had varied history of exposure to other common infections in this region (19–21, 25). In order to study the

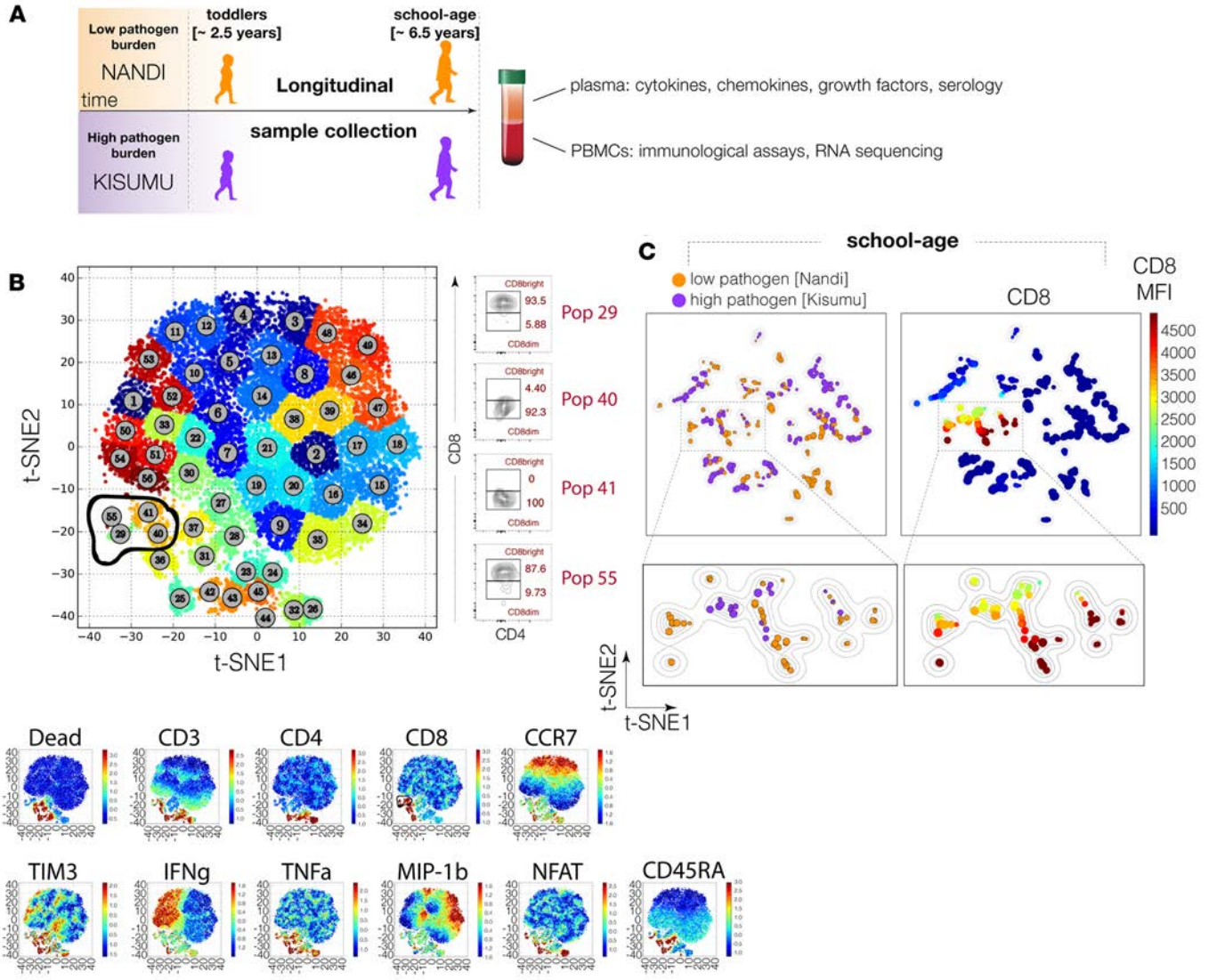

Figure 1. Children with elevated pathogen burden exhibit a distinct CD8⁺ T cell immune profile. (**A**) Schematic diagram summarizing the study design: peripheral blood mononuclear cells (PBMCs) were collected from Kenyan children residing in Kisumu (high malaria burden) and Nandi (low malaria burden) at ~2.5 years of age and at ~6.5 years of age. (**B**) Isolated PBMCs were stained with antibodies and analyzed by flow cytometry. Depicted is a representative *t*-distributed stochastic neighbor embedding (t-SNE) plot generated by ACCENSE after dimensionality reduction and unsupervised clustering of flow cytometry data on unstimulated cells. Main image: cluster numbers (defined by markers combination and expression level; dots of identical colors belong to the same cluster). Right panel: representative t-SNE plot of CD8⁺ T cell clusters displaying CD3⁺ $CD8^{bright}$ and $CD8^{dim}$ cells identified as clusters 29, 40, 41, and 55. Images below: representative heatmaps depicting the expression level of each marker and spatial localization on the t-SNE map. (**C**) Megacluster image of flow cytometry data performed by PhenoGraph showing malaria burden and CD8 surface expression (mean fluorescence intensity [MFI] scale) on a population level. Displayed here are unstimulated PBMC vials from school-age children living in Nandi (orange) and Kisumu (purple). Each dot represents a cluster, and the size of the dot represents the frequency of cells in the cluster. Surface CD8 expression (MFI) is displayed on heatmap scale on the right. Image generated from 5 independent experiments.

history of past infections within our study participants, we assessed cumulative pathogen burden by measuring antibodies (IgG) directed against select liver- and blood-stage malaria antigens, EBV, and Sm, along with antibodies to vaccine antigens (tetanus toxoid and edmonston measles vaccine virus) (Supplemental Figure 1). Unsupervised clustering of serological data revealed coclustering of school-age children consistent with their geographic origin, suggesting that antibody titers reflect expected cumulative pathogen exposure. In contrast, toddlers displayed greater heterogeneity within study groups that was poorly associated with place of residence and prevalence of infectious diseases characteristic of the region (Figure 3A). This suggests that putative exposures attributed to residing in Kisumu or Nandi, defined as an ecological variable, may not be informative to characterize cumulative exposures

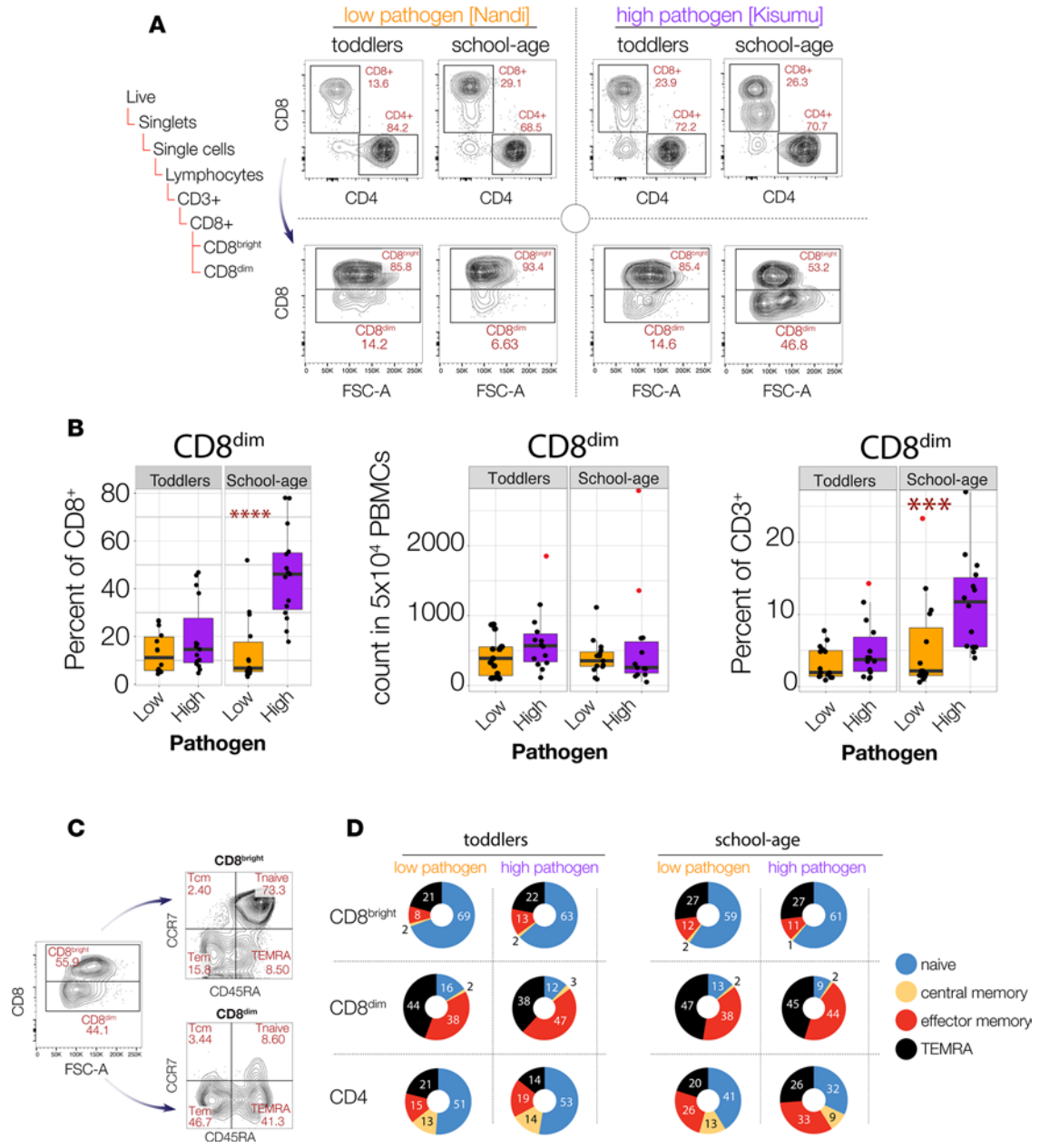

Figure 2. Cumulative pathogen burden promotes the development of CD3⁺ CD8^{dim} T cells. (**A**) Gating strategy and representative bivariate plot of unstimulated PBMCs from Nandi and Kisumu. FSC, forward scatter. (**B**) Boxplot (median and 95% interquartile range [IQR]) representing the proportion and the absolute count of CD8^{dim} T cells in Nandi (n=14) and Kisumu (n=15) children. Black dots on boxplot represent individual patients. Outlier values are indicated with red dots. The median proportion of CD8^{dim} T cells (percent CD8⁺ T cells) were as follows: Nandi = 6.7%, Kisumu = 46.1% with a significance level ***$P < 0.001$, ****$P < 0.0001$ (two-tailed unpaired *t* test with Welch's correction). (**C**) Representative bivariate plot displaying flow cytometry gating of CD3⁺ CD8⁺ T cell functional subsets. (**D**) Pie charts showing the proportion of CD8⁺ and CD4⁺ T cell subsets comparing the same children over time from Nandi and Kisumu. Data accumulated from 9 independent experiments, $n = 14$ (Nandi), $n = 15$ (Kisumu). The proportion of T cell subsets are different between CD8^{bright} and CD8^{dim} but not over time (Welch's *t* test).

for children at such a young age, and it suggests that interspersed longitudinal sample collection may miss detection of transient or subpatent infections. Not surprisingly, clusters in school-age children were driven by Pf and EBV antibody titers and were in accordance with previous studies (19, 25). Interestingly, we found that, in school-age children, antibody titers for Pf and Sm were positively correlated with the percentage of CD8^{dim} T cells (Figure 3B), while antibody titers to EBV antigens, measles vaccine virus, or tetanus toxoid were not.

Children living in areas of high pathogen burden have significantly elevated levels of plasma soluble CD163. Next, we examined the cytokine profiles in these children to determine if cytokine milieu was associated with the increased proportion of $CD8^{dim}$ T cells. We used multiplex panels to measure 51 plasma analytes (IL-1β, IL-1ra, IL-2, IL-4, IL-5, IL-6, IL-7, IL-8, IL-9, IL-10, IL-12(p70), IL-13, IL-15, IL-17, Eotaxin, FGF basic, G-CSF, GM-CSF, IFN-γ, IP-10, MCP-1, MIP-1α, PDGF-BB, MIP-1β, RANTES, TNF-α, VEGF, APRIL, BAFF, sCD30, sCD163, Chitinase 3-like 1, gp130, IFNβ, IL-11, IL-19, IL-20, IL-26, IL-27, IL-28, IL-29, IL-32, IL-34, IL-35, LIGHT, Osteocalcin, Pentraxin-3, sTNF-R1, sTNF-R2, TSLP, TWEAK). After adjusting for multiple comparison on the 51 analytes, we found that the increased proportion of $CD8^{dim}$ T cells was neither associated with a steady-state type 2 polarizing environment as reported in mouse models (32, 35), nor with differential expression of IL-10, IL-12, or TGFβ (data not shown). Instead, we discovered that children living in areas of high pathogen burden had significantly higher levels of soluble CD163 (sCD163) in their plasma (Figure 3C). sCD163 (a hemoglobin-haptoglobin scavenger receptor solely expressed on monocytes and macrophages) is released in the plasma upon activation via TLR ligation and serves as a biomarker for macrophage activation (36–39). Consequently, elevated levels of sCD163 observed in the plasma of Kisumu children, likely due to high pathogen burden (mainly malaria and schistosomiasis), might affect several branches of the immune system during infection, resulting in the generation of atypical cell subsets such as $CD8^{dim}$ T cells.

$CD8^{dim}$ T cells represent a transcriptionally and functionally distinct state of $CD8^+$ T cells. Due to limitations in blood volumes obtainable from children, we decided to first examine transcriptional profiles comparing $CD8^{bright}$ with $CD8^{dim}$ T cell subsets in PBMCs collected from adults with different histories of malaria exposure. $CD8^{dim}$ T cells were found to a greater degree in healthy adult Africans (44.2% median, $n = 11$) and to a much lesser extent in malaria-naive North Americans (8.2% median, $n = 9$) (Figure 4A), suggesting that this $CD8^+$ T cell stratification was not restricted to Kenyan children but may represent a distinct cell subset that persists into adulthood after cumulative pathogen exposure. Both $CD8^{bright}$ and $CD8^{dim}$ T cells had comparable viability potential, as only 3% of $CD8^{dim}$ T cells were Caspase 3–positive compared with none within the $CD8^{bright}$ T cell subset (Figure 4B). Analysis of the proliferative potential upon stimulation with anti-CD3 and anti-CD28 antibodies for 72 hours of sorted $CD8^{dim}$ T cells, and $CD8^{bright}$ $CD45RA^+$ and $CD45RA^-$ T cells, from an adult individual previously exposed to malaria revealed that $CD8^{dim}$ T cells had stunted proliferation compared with $CD8^{bright}$ T cells (for both $CD45RA^+$ and $CD45RA^-$ subsets). Of note, after 96 hours of stimulation, a subset of $CD8^{dim}$ cells appeared to upregulate CD8α expression (Figure 4C), suggesting a contextual plasticity in $CD8^{dim}$ T cells. Furthermore, we observed that $CD8^{dim}$ T cells from Kenyan school-age children and Kenyan adults, as well as from North American adults, were essentially αβ and not γδ T cells with a limited proportion of cells expressing surface CD56 (Supplemental Figure 2).

To better characterize these $CD8^+$ T cell subsets, we performed mRNA sequencing on sorted $CD8^{bright}$ and $CD8^{dim}$ T cells, further gated into CD45RA and CCR7 subsets, collected from 3 healthy adults representing diverse cumulative pathogen-exposure histories. Although all functional subsets of $CD8^+$ T cells shared a set of differentially expressed genes determined after unsupervised clustering analysis (Figure 5A), we found that T_{EM} and T_{EMRA} contained the most differentially expressed genes when stratified as $CD8^{dim}$ or $CD8^{bright}$ (Figure 5, B and C). $CD8^{dim}$ T cells were not only characterized by differentially expressed genes involved in innate-like functions (Figure 6A), but they also were highly enriched in TNFα, NF-κB, and IL-6 signaling pathways when compared with total $CD8^{bright}$ T cells after gene set enrichment analysis (GSEA) (Figure 6B). Altogether, our data show that $CD8^{dim}$ T cells are transcriptionally distinct from $CD8^{bright}$ T cells.

High pathogen burden promotes the development of Granzyme $B^+IFNγ^{low}TNFα^{low}CD3^+CD8^{dim}$ T cells. In order to validate transcriptional differences between $CD8^{bright}$ and $CD8^{dim}$ T cells subsets, we returned to samples from our Kenyan school-age cohorts and selected significantly differentially expressed genes that had commercially available antibodies for flow cytometry (Figure 7). While $CD8^{bright}$ T cells from high- and low-pathogen toddlers showed comparable proportions of T cells subsets (Figure 2D), $CD8^{dim}$ T cells from high-pathogen toddlers displayed significantly higher proportions of IFNγ, TNFα, and CCL4-producing cells upon in vitro stimulation with staphylococcal enterotoxin B (SEB) (Figure 7A). Interestingly, $CD8^{dim}$ T cells from these high pathogen–burden children (4 years later) developed severely impaired CCL4 and IFNγ production and displayed substantially decreased proportions of functional effector cells in both $CD8^{bright}$ and $CD8^{dim}$ compartments. Strikingly, and contrasting with some murine observations (32), we found that $CD8^{dim}$ T_{EM} and T_{EMRA} had significantly elevated levels of Granzyme B in steady state, which is reminiscent of ILC1s and type-1 innate-like T cells (ILTC1s) developing in the context of tumor-elicited immune surveillance (24) (Figure 7, B and C).

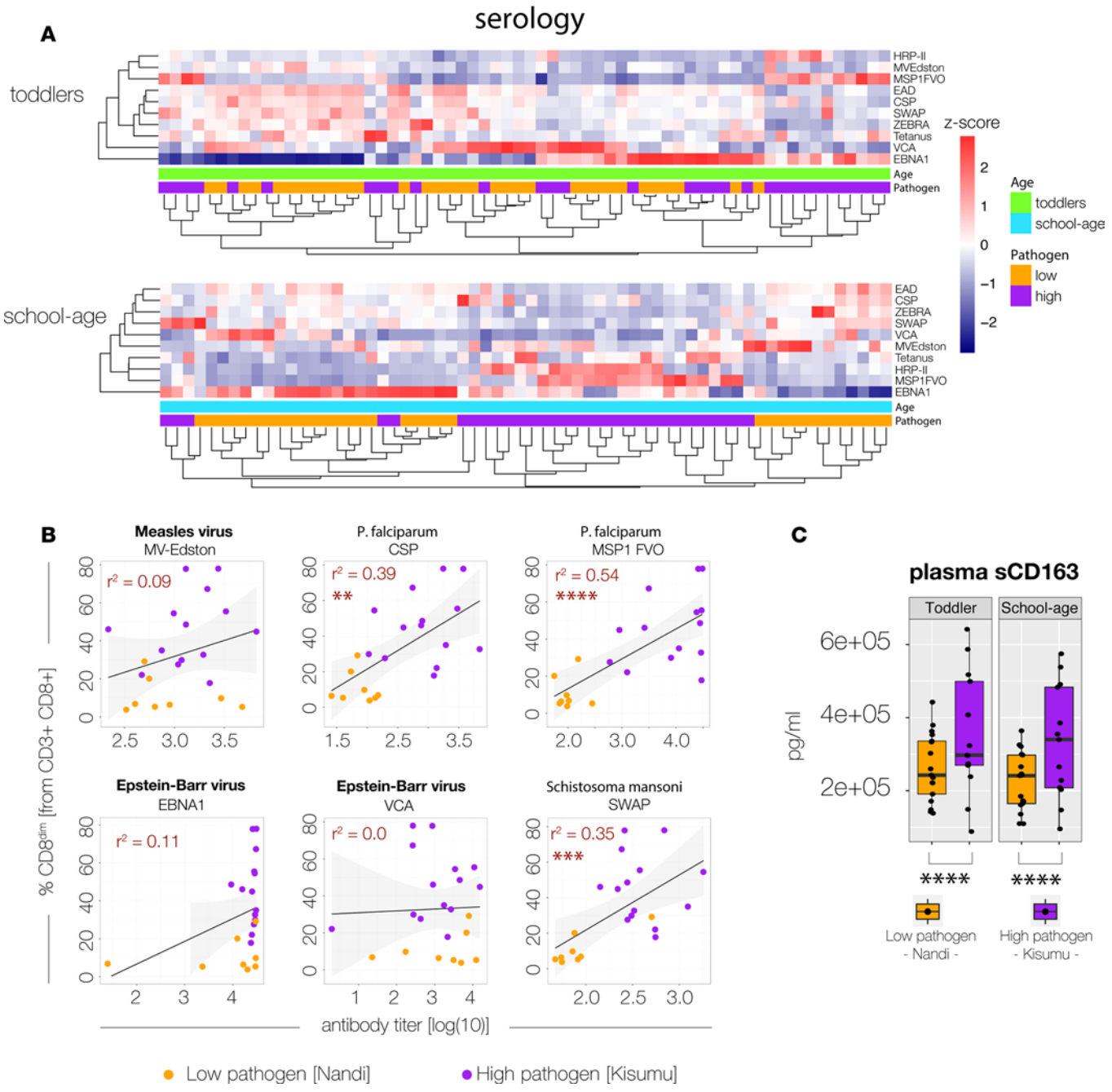

Figure 3. Children living in areas of elevated pathogen burden develop distinctive serological and plasma cytokine profiles. Serum antibody titers and plasma analytes were measured at a 4-year interval (toddlers to school-age) coinciding with T cell subset assays. Immunity to vaccine antigens, measles, and tetanus were measured as controls (Nandi, n = 33; Kisumu, n = 31). Antibody titers (IgG) specific for Pf (HPR-II, MSP1-FVO, CSP), measles virus (edmonston vaccine strain), Clostridium tetani (tetanus), Schistosoma mansoni (SWAP), and EBV (EAD, ZEBRA, VCA, EBNA1) were measured using multiplex conjugated-bead suspension assay. (**A**) Heatmap of scaled antibody titers (Z score). Pathogen burden is represented with orange (low, Nandi) and purple (high, Kisumu). Data generated from 1 experiment measuring plasma antibody titers from patients. (**B**) Dotplots (and 95% CI) representing the association between proportion of $CD3^+$ $CD8^{dim}$ T cells and pathogen-specific antibody titers in school-age children. Solid lines represent best-fit regression line and coefficient of determination (r^2), and P values are displayed (*P < 0.05, ***P < 0.001, ****P < 0.0001). (**C**) Steady-state plasma sCD163 levels from toddlers and school-age children. Boxplot (median and 95% IQR) displays the relative amount of sCD163 (pg/ml) (Nandi, n = 14; Kisumu, n = 15). Black dots are values from individual children. Two-way ANOVA with Sidak multiple comparison post test was used to analyze statistical significance for the 51 analytes measured in the two groups of divergent pathogen exposure. Data generated from one experiment measuring plasma analytes titers from 29 patients.

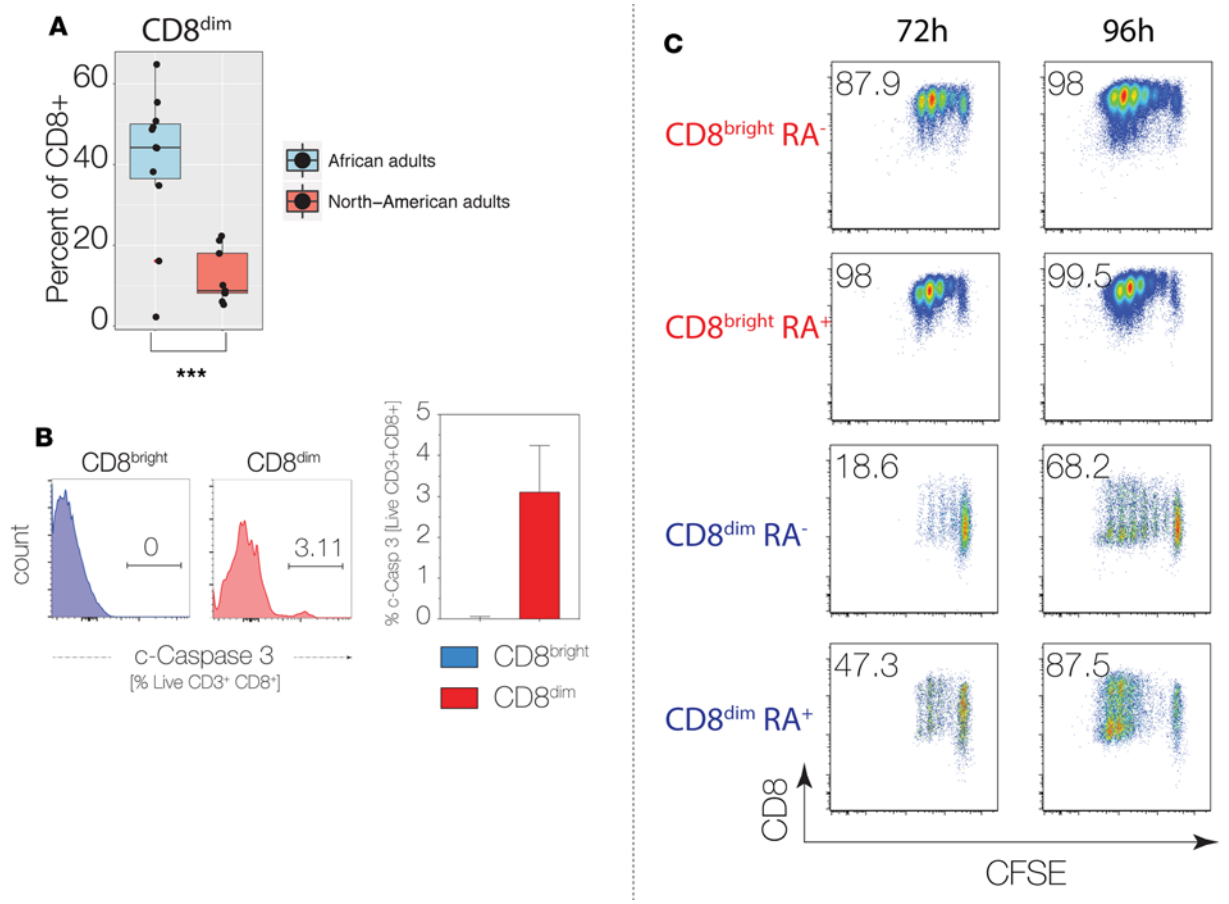

Figure 4. Healthy African adults have greater proportions of CD3⁺ CD8^{dim} T cells than healthy North American adults. (**A**) Peripheral blood mononuclear cells (PBMCs) were stained with a panel of fluorescently labeled antibodies to define T cell subsets and then analyzed by multiparameter flow cytometry. Data on the boxplot (median and 95% IQR) display the proportion of CD8^{dim} T cells from healthy Kenyan adults (n = 11) and healthy North American adults (n = 9). Computed two-tailed unpaired t test with Welch's correction P value is displayed at the bottom of the graph (***$P < 0.001$). Black dots on the boxplot display values from individual healthy adults. Data generated from 1 flow cytometry experiment. (**B**) Caspase 3 was detected in ~3% of CD8^{dim} and not in CD8^{bright} T cells, indicating that neither cell population is undergoing apoptosis. (**C**) Representative flow cytometric analysis of CFSE-labeled profile of CD8^{bright} and CD8^{dim} T cells, either CD45RA⁺ or CD45RA⁻ sorted from the peripheral blood of an adult sample that had previously been exposed to malaria. Cells were analyzed after 72 and 96 hours of stimulation with α-CD3 and α-CD28 antibodies. The number in each plot represents the percentage of cells that proliferated.

CD8^{dim} T cells from school-age children living in areas of high pathogen burden have low NFAT1. In addition to having graded levels of NFAT1 (a key transcription factor involved in TCR signaling) in CD8⁺ T cells subsets, we found that cumulative pathogen burden negatively affected NFAT1 levels (Figure 8, A and B). In fact, decreased NFAT1 in addition to low surface CD8 expression is consistent with the defect in T cell effector function observed in school-age children from high-pathogen areas. In general, our data show that CD8^{bright} T cells expressed higher levels of CXCR4, ABCB1, CD11a, KLF2, KLRK1, and CD2 compared with CD8^{dim} T cells (Supplemental Figure 3A). Interestingly, the expression levels of some of these markers seemed to be independent of cumulative pathogen burden, as school-age children from both areas displayed varied expression (Supplemental Figure 3B). In addition, we examined transcriptional regulators of T cell differentiation (40) and found that high pathogen–exposure children had severely diminished frequencies of T_{EM} and T_{EMRA} CD8⁺ T cell subsets coexpressing the transcription factors T-bet and Eomesodermin (Eomes) compared with their age-matched, low pathogen burden counterparts (Figure 9). Taken together, our data demonstrate that parasitic infections during childhood induce transcriptional changes in CD8⁺ T cells favoring an innate-like circuitry of transcription factors and a pronounced steady state biosynthesis of Granzyme B.

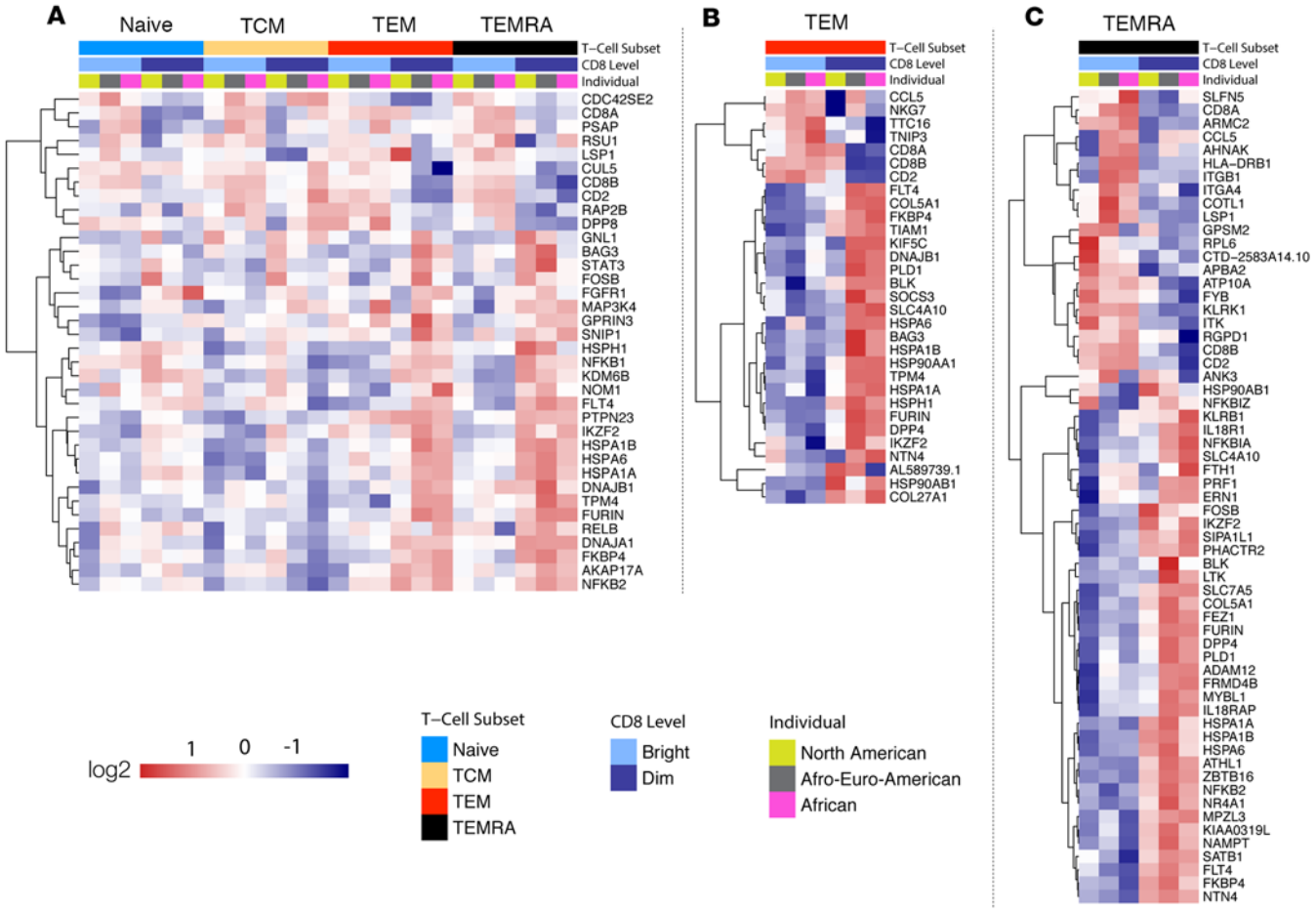

Figure 5. CD3$^+$ CD8^{dim} T cells represent a transcriptionally distinct subset of human CD8 T cells. RNA sequencing was performed on sorted CD8$^+$ T cell subsets from 3 healthy adult donors with different histories of cumulative exposure to pathogen (North America/USA, low pathogen burden; Africa, perennial pathogen burden; and Africa-Europe-USA, quondam pathogen burden). Heatmap display significantly differentially expressed genes (Benjamini-Hochberg method [BH] $P_{adj} < 0.1$). (**A**) List of differentially expressed genes obtained after unbiased comparison of genes shared by the 4 CD8$^+$ T cell subsets defined by CCR7 and CD45RA in CD8^{bright} and CD8^{dim}. Differentially expressed genes between CD8^{dim} and CD8^{bright} cells in (**B**) T_{EM} and (**C**) T_{EMRA}. Data generated from 1 experiment.

Discussion

Using a prospective cohort study of children exposed to different intensities of infectious diseases from 2–7 years of age, we were able to characterize their influence on the development of T cell subsets. We included malaria, Schistosomiasis, and EBV as exposures and observed an expansion of unconventional CD8^{dim} T cells displaying innate-like characteristics (Granzyme B^{hi}, IFNγ^{low}, TNFα^{low}, PLFZ^{hi}, ID2^{hi}, IKZF2^{hi}), reminiscent of NK cells and ILC1 (22–24) that develops in otherwise healthy children residing in areas of high pathogen burden. In contrast, longitudinal assessments of age-matched Kenyan children from a highland area with low pathogen burden showed that these children developed a more conventional polyfunctional IFNγ$^+$, TNFα$^+$, CCL4$^+$CD3$^+$CD8^{bright} T cell profile as they aged. The fact that CD8^{dim} T cells persisted into adulthood when there was a history of elevated pathogen burden and that their frequencies were largely associated with a maturing immune system for children in the face of cumulative pathogen burden suggests their potential contribution to protection from disease. Our study participants were in general good health; therefore, we speculate that CD8^{dim} T cells may be an adaption consistent with premunition, thereby protecting an individual from immunopathology. However, future studies would be needed to determine if CD8^{dim} T cells are directly involved in pathogen clearance or protection from infection, or if they are the result of immune tolerance mechanisms.

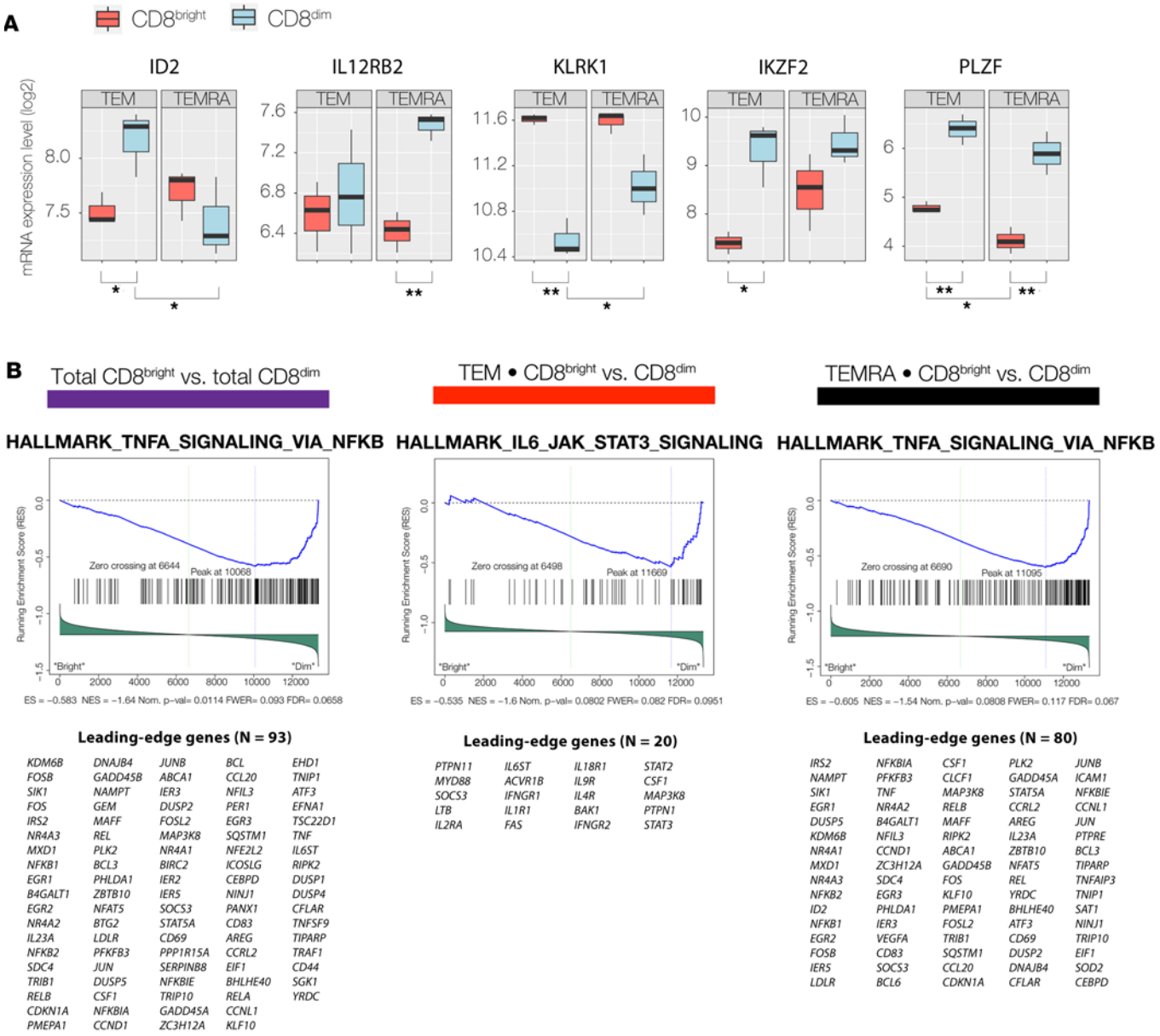

Figure 6. CD3⁺ CD8^{dim} T cells display an atypical transcriptome signature reminiscent of type 1 innate lymphoid cells. RNA sequencing was performed on sorted CD8⁺ T cell subsets from 3 healthy adult donors with different histories of cumulative exposure to pathogen (North America/USA, low pathogen burden; Africa, perennial pathogen burden; and Africa-Europe-USA, quondam pathogen burden). (**A**) mRNA expression level of ID2, IL12RB2, KLRK1, IKZF2, and PLZF in T_{EM} and T_{EMRA}. Computed two-tailed Welch's *t* test *P* values are displayed (*$P < 0.05$, **$P < 0.01$). (**B**) Gene set enrichment analysis (GSEA) comparing enriched pathways in total CD8^{bright} and CD8^{dim}, T_{EM}, or T_{EMRA} from CD8^{bright} and CD8^{dim}. The list of leading genes in each enriched pathway is provided; genes are ranked by their enrichment score (highest to lowest). Data generated from 1 experiment.

Consistent with our findings are reports that CD8⁺ T cells expressing Granzyme B have been identified as mediators of cerebral malaria in mouse models (41, 42). In contrast to contributing to immunopathology, Granzyme B produced by CD8⁺ and γδ T cells in experimental, controlled human malaria infections (CHMI) are associated with protection from liver-stage infection (41–44). Within the context of a CHMI study, adults from Tanzania that were preexposed to malaria were unable to produce IFNγ recall responses from CD8⁺ and γδ T cells, compared with malaria-naive Dutch adults (45). Even though Granzyme B levels were not measured, IFNγ levels were low prior to sporozoite challenge.

Although downregulation of CD8 coreceptor is often subsequent to TCR-mediated signaling (46), a significantly high proportion of CD8^{dim} T cells has been observed in African green monkeys (AGM) and was protective against SIV infection (47). Furthermore, in some contexts, CD8^{dim} T cells substituted for CD4⁺ T cells and

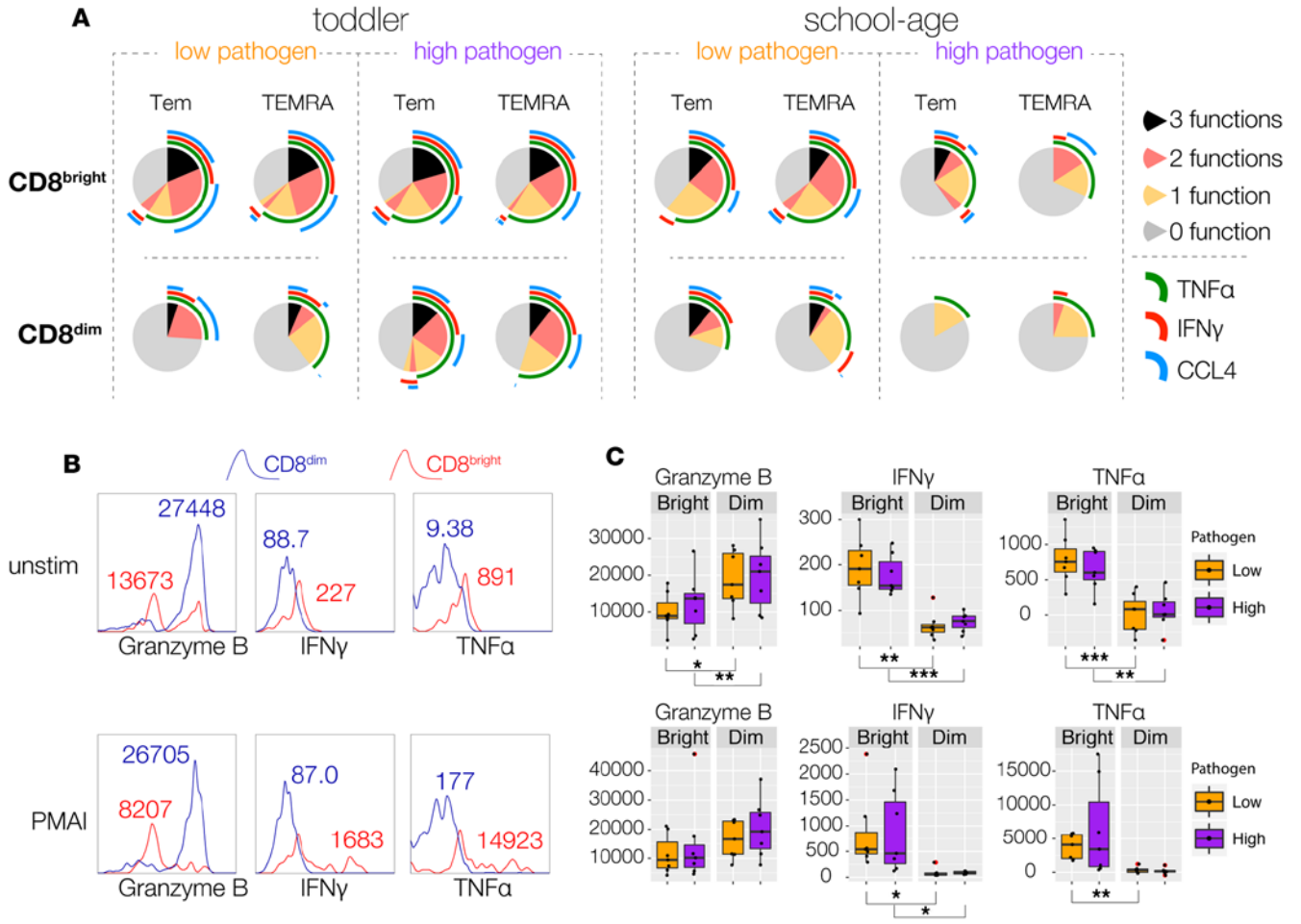

Figure 7. Atypical Granzyme B$^+$ IFNγ^{low} TNFα^{low} CD3$^+$ CD8^{dim} T cells arise in school-age children living in areas of high pathogen burden. (**A**) PBMCs were stimulated with Staphylococcus enterotoxin B (SEB) in vitro for 4 hours, and cytokines were measured in T_{EM} and T_{EMRA}. Pie charts generated with SPICE (Simplified Presentation of Incredibly Complex Evaluations) representing qualitative response of CD8^{bright} and CD8^{dim} T cells using Boolean combination of gates identifying TNFα, IFNγ, and CCL4 (MIP-1β). Pie chart colors represent number of effector molecules, while each cytokine is represented by an arc (Nandi, n = 14; Kisumu n = 15). (**B**) Representative histograms of T_{EM} cells gated for Granzyme B, IFNγ, or TNFα from unstimulated and PMA/ionomycin-stimulated CD8$^+$ T cells (4 hours). (**C**) Boxplots of computed MFI from **B** (Nandi, n = 8; Kisumu, n = 8). Welch's two-tailed t test P values are displayed (*P < 0.05, **P < 0.01, ***P < 0.001). Black dots on boxplot represents individual patients. Outlier values are indicated with red dots. Data generated from five independent experiments.

provided B cell help, leading to antibody production (48, 49). Other studies showed that type 2 polarization of CD8$^+$ T cells induced epigenetic modifications on the CD8α locus, resulting in downregulation of CD8 surface expression in mice (32). That phenotype was sustained in vivo following adoptive transfer and was partially reversed in the presence of IFNγ (35). Altogether, our findings and these previous studies suggest that CD8^{dim} T cells are not simply activated CD8$^+$ T cells with downregulated CD8 coreceptors, but instead represent a cell state dynamically arising from a specific immunological context.

A limitation to human immunology studies is that conclusions are of necessity derived from circulating PBMCs from living study participants. Recent studies of organ donors elegantly demonstrate that the composition of human immune cells varies with their tissue localization, suggesting that immunological findings resulting from human PBMCs should be interpreted very cautiously (5, 6). Regardless of this understandable criticism, our longitudinal childhood cohort study was able to demonstrate remarkable differences in CD8$^+$ T cell subsets associated with prolonged pathogen exposure, notably to malaria and Schistosomiasis. The role of Schistosomiasis in shaping human T cell lineage and fate decisions is speculative at this stage, but Schistosomiasis has been shown to activate CD8$^+$ T cells (50). Additionally, the distinctive plasma composition observed in the Kisumu compared with the Nandi children displays another layer of complexity generally overlooked in human immunology studies. Generally, very few in vitro assays conducted with human PBMCs replicate

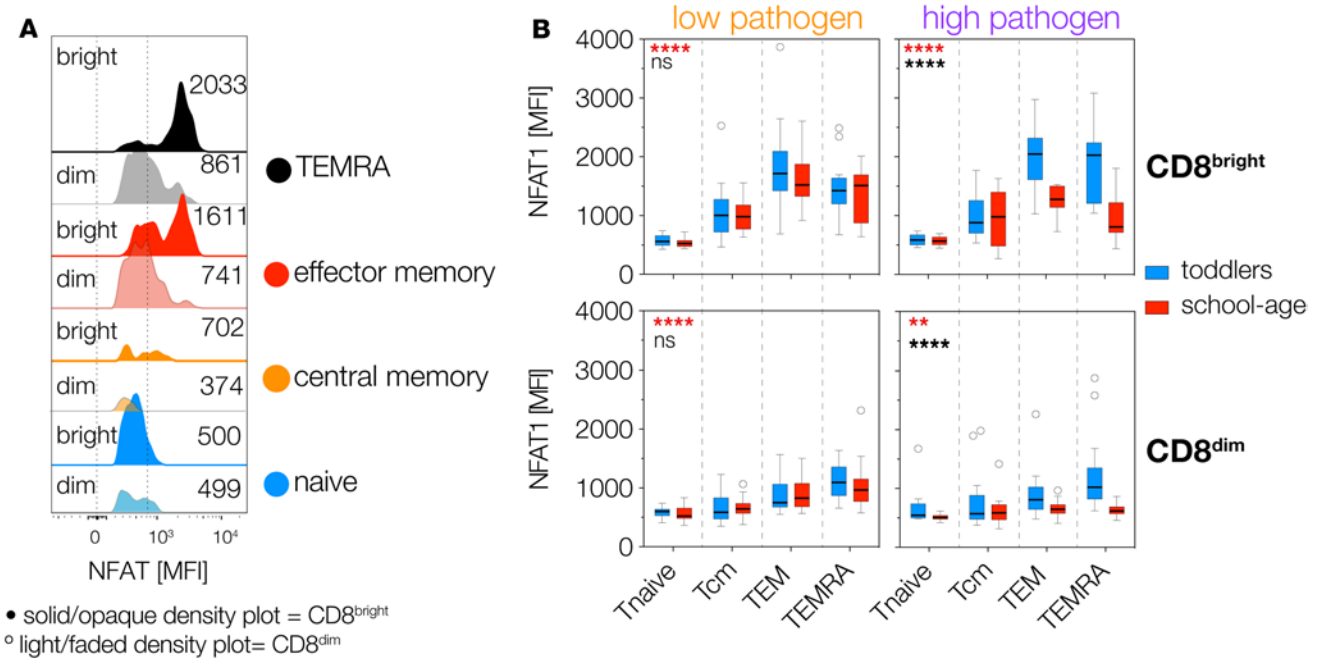

Figure 8. CD3⁺ CD8^{dim} T cells from school-age children living in areas of high pathogen burden have low NFAT1. Unstimulated PBMCs from Nandi and Kisumu (low and high pathogen burden areas, respectively) were fluorescently labeled and analyzed with flow cytometry. (**A**) Representative histograms displaying graded NFAT1 in unstimulated CD8⁺ T cell subsets. (**B**) Boxplot (median and 95% IQR) representing computed MFI of NFAT1 in toddlers and school-age children (Nandi, $n = 14$; Kisumu, $n = 15$). Two-way ANOVA (**$P < 0.01$, ****$P < 0.0001$) comparing the amount of NFAT1 protein levels in CD8⁺ T cell subsets (red asterisks) or in paired samples from toddlers and school-age (black asterisks). Data generated from five independent experiments.

the impact of plasma cytokine found in the patient when interrogating the function of immune cells ex vivo. Further investigations are warranted to dissect not only what pathogen-induced mediators drive the observed plasma cytokine composition, but also to elucidate the long-term effects of the cytokine microenvironment on immune cell homeostasis and function in these children.

Structural and functional constituents of the human immune system are dynamically regulated in response to developmental and environmental cues (6, 14, 15, 46). Here, we have identified a subpopulation of CD8⁺ T cells with a distinct transcriptional profile showing significant expansion in individuals repetitively infected with parasites; it may represent a dynamic cell state in CD8⁺ T cell biology resulting from an adaptation of the immune system in response to persistent pathogen exposure, rather than reflecting a fixed cell type. In fact, although this subpopulation expressed detectable protein levels of CD3 and CD8, their transcriptome and in vitro stimulation signature suggest severely impaired TCR signaling (low CD2, CD8, ITK, NFAT1) in favor of an innate-like circuitry (high PLZF, ID2, IKZF2, Granzyme B) (22–24, 51). Our observations as well as recent publications (22–24) emphasize the study of immune cells as dynamic entities adapting to the microenvironment rather than classify them with a static set of cell surface markers that might merely reflect their status at the time of analysis.

While the chemokine receptor CXCR4 and the transcription factor KLF2 regulate T cell migration and memory formation (52–56), their downregulation is one of the hallmarks of ILC1s and ILTC1s (24). CD8^{bright} and CD8^{dim} T cells are not only metabolically dissimilar as described in murine studies (57, 58), but they may also have significantly distinct migratory and memory potential. Furthermore, while CD8⁺ T_{EM} and T_{EMRA} cells from school-age children living in Kisumu showed no exhaustion phenotype compared with Nandi children (as determined by Tim-3 expression; Figure 1B and Supplemental Figure 4), they predominantly coexpressed T-bet and Eomes at similar levels regardless of cell subset (Figure 9, C and D), an expression pattern often observed during NK maturation (59). This may suggest that these are short-lived effector cells, which would be consistent with mouse models (60), or alternatively that T-bet and Eomes ratios are not informative to predict CD8⁺ T cell fate in humans. More in-depth, longitudinal human immunology studies are necessary in order to fully explore transcriptional regulation of T cell differentiation and the relevance to protection from acute and chronic infections.

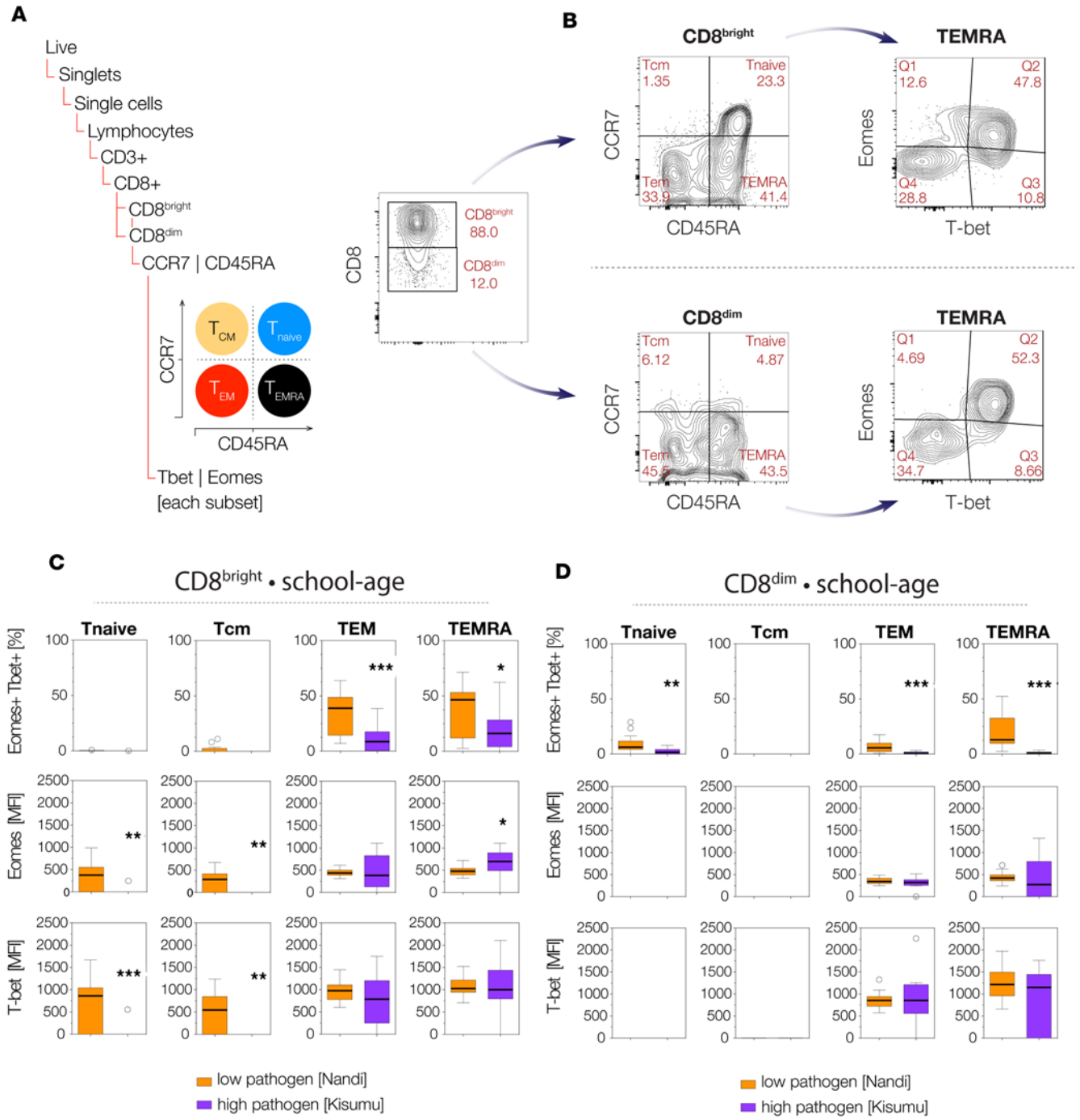

Figure 9. School-age children from Kisumu (high pathogen burden) have lower proportions of CD8⁺ T_{EM} and T_{EMRA} cells coexpressing T-bet and Eomes transcription factors compared with Nandi (low pathogen burden). Peripheral blood mononuclear cells (PBMCs) were stained with antibodies to define T cell subsets and effector functions and then analyzed by multiparameter flow cytometry. (**A**) Gating strategy and (**B**) bivariate flow cytometry density plot displaying the proportion of CD8⁺ T cell subsets expressing T-bet and Eomes transcription factors. (**C** and **D**) Boxplots (median and 95% IQR) displaying the proportion of $CD8^{bright}$ and $CD8^{dim}$ T cell subsets coexpressing T-bet and Eomes from school-age children from Nandi (low pathogen burden, $n = 14$) and Kisumu (high pathogen burden, $n = 15$). Computed two-tailed unpaired t test with Welch's correction P values are displayed on each graph (*$P < 0.05$, **$P < 0.01$, ***$P < 0.001$).

It is possible that the population of unconventional $CD8^{dim}$ T cells are NKT-like cells expressing low levels of CD8α (61). However, our data do not support this hypothesis, since we did not observe a significant difference in CD56 mRNA or protein expression between $CD8^{bright}$ and $CD8^{dim}$ T cells (Supplemental Figure 2, C and F, and data not shown). Altogether, our findings suggest that $CD3^{+}CD8^{dim}$ Granzyme

$B^+IFN\gamma^{low}TNF\alpha^{low}$ T cells represent a distinct cell program in human $CD8^+$ T cell biology. Further studies will elucidate their contribution in chronic diseases and cancer immunosurveillance, and their relevance to observed variation in vaccine efficacy in different populations.

Methods

Study design. We enrolled 140 children from the infant cohort previously described (19, 25) when they reached 2.5–3 years of age. Of those, we had 70% retention over the 4-year study period, until the age of 6.5–7 years. This was a normal, gradual rate of attrition expected for a longitudinal pediatric cohort study of healthy children. Those who continued to participate were not more or less likely to have been ill during the course of the study, aside from differences in episodes of uncomplicated malaria experienced in Kisumu children in contrast with children from Nandi. From those children with complete datasets, we randomly selected the subset for this immunologic study. For the current immunologic study, toddlers (2.4–3.5 years old) from Kisumu (n = 31), a high malaria transmission area on the shores of Lake Victoria, which is known to be a source of Sm (62) infections (high pathogen burden area) and Nandi (n = 33), a highland area with little malaria and no Schistosomiasis (low pathogen burden area) were followed prospectively until school age (5.5–6.5 years old). Healthy adult donors from Kisumu (n = 11) and the USA (n = 9) were also enrolled. Only HIV-negative individuals were enrolled.

PBMC isolation. PBMC collected in sodium heparin anticoagulated vacutainer tubes (BD Biosciences) were isolated using Ficoll-Hypaque gradient centrifugation. PBMCs were cryopreserved in 10% DMSO (90% heat-inactivated FBS). Plasma fractions were also collected. Samples were shipped from Kenya to the USA maintaining the cold chain. Cells were thawed and rested overnight in a 5% CO_2 incubator (Forma Scientific - Co2 Water Jacketed Incubator), and viability was checked prior to commencing experiments.

Multiplex bead-based assays (Bioplex). Luminex bead–based multiplex immunoassay was used to simultaneously measure plasma antibody titers using previously published methods (25). In brief, recombinant proteins or synthetic peptides covering epitopes of Pf antigens (preerythrocytic-stage antigens CSP, CelTos, LSA1, and rPfSEA-A1; blood-stage antigens AMA1 [FVO], HRP-II, MSP1 [FVO, 3D7, FUP]; edmonston measles vaccine virus; tetanus toxoid; Sm worm antigen protein [SWAP]; and EBV antigens EAD, ZEBRA, VCA, EBNA1, BHFR1 p17 [otp 359, 360, 364])were conjugated to beads to detect pathogen-specific antibodies following manufacturer's instructions (Bio-Rad). Antigens were gifts from Jaap Middeldorp (VU University Medical Center, Amsterdam, The Netherlands) for EBV serology profiles, Greg Poland and Inna Ovsyannikova from the Mayo Clinic (Rochester, Minnesota, USA) for the Measles Vaccine virus extract, Evelina Angov and Sheetij Dutta at Walter Reed Army Institute of Research (Silver Spring, Maryland, USA) for malaria recombinant proteins, and Jonathan Kurtis at Rhode Island Hospital for the Schistosome (Brown University, Providence, Rhode Island, USA) worm antigen preparations and malaria rPfSEA-A1.

Plasma cytokines, chemokines, and growth factors were measured using Bio-Plex Pro Human Cytokine 27-plex Assay (Bio-Rad, M500KCAF0Y) and Pro Hu INF Panel 1 24-Plex (Bio-Rad, 171AL002M) according to manufacturer instructions. Plasma was thawed on ice, filtered, and diluted prior to being run on the Bio-Rad platform.

Relative antibody titers were scaled (Z score normalization) for heatmap generation using R statistical packages. Spearman coefficient of correlation r between $CD8^{dim}$ and antibody titers, as well as statistical significance of antibody titers between children from low pathogen and high pathogen burden, was calculated with GraphPad PRISM using Welch's Student t test assuming unequal variances. Statistical significance and data visualization were calculated with GraphPad PRISM and R statistical packages (CRAN).

Flow cytometry analysis. The following reagents were used to assess cell viability: live/dead aqua (Invitrogen, L34957) and cleaved Caspase-3 (Alexa Fluor 488, Cell Signaling Technologies). The cell staining method is a modified version of Lugli et al. protocol (63). The following fluorochrome-conjugated antibodies were used for surface staining: anti-human CD2 (BB515, RPA-2.10, BD Biosciences), CD3 (PE-Cy5, BD Biosciences), CD4 (PE-Texas Red, S3.5, Invitrogen), CD8 (Pacific Blue, RPA-T8, BD Biosciences), CD11a (FITC, BioLegend), CD45RA (PE-Cy7, L48, BD Biosciences), CD366/Tim3 (BV650, 7D3, BD Biosciences), ABCB1 (APC, UIC2, BioLegend), CCL4/MIP1β (APC, D21-1351, BD Pharmingen), CCR7 (PerCP-Cy5.5, 150503, BD Pharmingen), CXCR4 (APC-Cy7, 12G5, BioLegend), KLRK1 (APC-Cy7, 1D11, BioLegend). Intracellular staining was performed following manufacturer instructions from fixation/permeabilization concentrate and diluent (eBiosciences). Surface-stained cells were fixed for

30 minutes at 4°C, washed twice in cold washing buffer, and stained 30 minutes at 4°C with the following antibodies: IFNγ (Alexa-Fluor 780, 4S.B3, eBiosciences), Granzyme B (PE, Invitrogen), KLF2 (PE, R&D Systems), NFAT1 (PE, 1:100, 14335, Cell Signaling Technologies), T-bet (FITC, eBio4B10, eBiosciences), Eomes (eFluor 660, WD1928, eBiosciences), TNFα (FITC, MAb11, eBiosciences). For the proliferation assay, sorted subsets of PBMCs were labeled with 1 M CFSE (Invitrogen) in PBS at 37°C for 8 minutes. Labeled cells were added to 96-well flat-bottom plates coated with plate-bound anti-CD3 (1 μg/ml) and anti-CD28 (2 μg/ml) (Invitrogen), at a concentration of 25,000 cells/well in 200 μl of RPMI (GIBCO) culture media supplemented with 2 mM glutamine, 1% (vol/vol) nonessential amino acids, 1% (vol/vol) sodium pyruvate, penicillin (50 U/ml) and streptomycin (50 g/ml), and containing 10% (vol/vol) HI human serum (GEMINI Bio-Products). Stained cells were acquired on a 4-laser LSRII SORP analytical flow cytometer (BD Biosciences) and analyzed using FlowJo software (Tree Star Inc.). Compensated FCS files from each experimental conditions were later used as input files for ACCENSE (27) and PhenoGraph.

Cell sorting and RNA sequencing. $CD8^+$ T cells were enriched from PBMCs (Stem Cell Technologies, 19053). Cells were stained with live/dead aqua (Invitrogen), propidium iodide (Invitrogen), CD3 (PE-Cy5, BD Biosciences), CD4 (PE-Texas Red, Invitrogen), CD8 (Pacific Blue, BD Biosciences), CCR7 (PerCP-Cy5.5, BD Pharmingen), and CD45RA (PE-Cy7, BD Pharmingen). Functional subsets defined by CCR7 and CD45RA stained were sorted in individual tubes from $CD8^{bright}$ and $CD8^{dim}$ T cells using a 4-laser BD FACSAria. Cells were collected in chilled 2× Buffer TCL with (2%) β-mercaptoethanol (Qiagen), and mRNA were isolated with oligo-dT using Dynabeads mRNA purification kit (Invitrogen). We followed standard protocol of SMARTer Stranded Total RNA-Seq Kit - Pico Input Mammalian for sequencing library preparation (Clontech). We performed the first-strand synthesis of purified mRNAs on Dynabeads using SMART pico oligos, which was followed by indexed Illumina Adapter ligation. We purified libraries using XP Ampure magnetic beads (Beckman Coulter Inc.) after each reaction step. Final libraries were amplified using SeqAmp DNA polymerase, and qualities were confirmed with a Bioanalyzer Agilent High sensitivity DNA kit and sequenced with paired-end read (2 × 100 bp) using an Illumina HiSeq 4000 (Illumina Inc.). Sequencing files were deposited in the NCBI's database of Genotypes and Phenotypes (dbGaP phs001282.v2)

Gene expression quantification and differential expression analysis. The qualities of raw sequencing reads were checked using FastQC (64). Multiplexed reads were sorted by sample based on unique sample indexes identified by Novobarcode (Novocraft Technologies). Residual Illumina adaptor sequences on the 3′ end and sequences of template switching oligos introduced during the cDNA synthesis were trimmed using Fastx Toolkit (65). After preprocessing, paired reads were aligned to a transcriptome index built by RNA-Seq by expectation-maximization (RSEM) (66) using Gencode annotation version 19 for protein coding transcripts and GRCh37/hg19 genomic sequence. RSEM calculated the expected read counts for each gene with strand-specific settings. We merged all possible isoform-specific counts into a union gene model, which has the longest transcript structure. Libraries were assessed from separate batches and/or sample collection with principal component analysis. To perform differential gene expression analysis, we used Bioconductor package DESeq2 (67), which fits the read counts to a negative binomial distribution and tests for significance using Wald test. After adjusting the *P* values for multiple testing with Benjamini-Hochberg procedure, genes that are differentially expressed between cell subsets were considered significant with 10% FDR cut off.

Gene set enrichment and pathway analysis. GSEA was performed on normalized expression data of subsets using the GSEA program (http://software.broadinstitute.org/gsea/index.jsp) (68). For a ranking metric, we used signal to noise value of each gene and performed a permutation test for FDR by permuting phenotype assignments 1,000 times. Gene sets examined included the gene sets of hallmark, oncogenic, and immunologic signatures, as well as the curated C2 gene sets such as Reactome and Kyoto Encyclopedia of Genes and Genomes (KEGG) pathways from the Molecular Signatures Database (MSigDB version 5.0 datasets; http://software.broadinstitute.org/gsea/msigdb/. A FDR *q* value less than 0.1 was used as a cutoff for inclusion.

Statistics. Statistical analyses and statistical significance for each group were computed using a two-tailed Student *t* test with Welch's correction for unequal variance (paired or unpaired). Two-way ANOVA with Sidak multiple comparison post test was used to analyze statistical significance for the 51 analytes measured in the two groups of divergent pathogen exposure. Significance levels are indicated as follows: $*P < 0.05$, $**P < 0.01$, $***P < 0.001$, and $****P < 0.0001$. Linear regression analysis, as well as all the aforementioned statistical analyses, were performed using GraphPad PRISM, SPICE Software (Simplified Presentation of Incredibly Complex Evaluations), and R statistical packages.

Study approval. This study was approved by the IRB at the University of Massachusetts Medical School, and the Scientific & Ethics Review Unit at the Kenya Medical Research Institute. Written informed consent was obtained from adult study participants and parents of minors prior to inclusion in the study.

Author contributions

YTF, YK, MF, JAB, LJB, and AMM designed the experiments; YTF, MF, and YK carried out the experiments, analyzed the data, and interpreted the results; JAB, LJB, CF, and AMM also contributed to the interpretation of the results; YTF, MF, and YK prepared the figures; AMM and JMO carried out the epidemiologic study design; YTF, YK, and JAB processed and analyzed transcriptome data; YTF wrote the manuscript; MF, YK, CF, JAB, LJB, and AMM edited the manuscript; and all authors read the manuscript and approved submission.

Acknowledgments

This work was supported by grants from the US NIH (CA134051 and CA189806 to AMM and AI099473 to JAB, UMCCTS Pilot Project Program U1 LTR000161 to AMM and JAB, and AI106833 to LJB) and the Turkish Ministry of National Education Graduate Study Abroad Program to YK. We would like to thank Rosemary Rochford for donating some of the early-age PBMC samples (NIH CA102667) (25), and we thank the children and their families for their participation in this study. We would also like to thank Joslyn Foley and Christina Nixon for assistance with sample management and generating the serology data. In addition, we thank the flow cytometry and genomics core facilities at the University of Massachusetts Medical School for their assistance in sorting the cells and performing mRNA sequencing, respectively. This manuscript was approved for publication by the Kenya Medical Research Institute.

Address correspondence to: Ann M. Moormann, 373 Plantation Street, Biotech 2, Suite 318, Worcester, Massachusetts 01605, USA. Phone: 508.856.8826; Email: ann.moormann@umassmed.edu.

1. Bevan MJ. Memory T cells as an occupying force. *Eur J Immunol*. 2011;41(5):1192–1195.
2. Masopust D, Picker LJ. Hidden memories: frontline memory T cells and early pathogen interception. *J Immunol*. 2012;188(12):5811–5817.
3. Dutton RW, Bradley LM, Swain SL. T cell memory. *Annu Rev Immunol*. 1998;16:201–223.
4. Mueller SN, Gebhardt T, Carbone FR, Heath WR. Memory T cell subsets, migration patterns, and tissue residence. *Annu Rev Immunol*. 2013;31:137–161.
5. Sathaliyawala T, et al. Distribution and compartmentalization of human circulating and tissue-resident memory T cell subsets. *Immunity*. 2013;38(1):187–197.
6. Thome JJ, et al. Spatial map of human T cell compartmentalization and maintenance over decades of life. *Cell*. 2014;159(4):814–828.
7. Day KP, Marsh K. Naturally acquired immunity to Plasmodium falciparum. *Immunol Today*. 1991;12(3):A68–A71.
8. Lindblade KA, Steinhardt L, Samuels A, Kachur SP, Slutsker L. The silent threat: asymptomatic parasitemia and malaria transmission. *Expert Rev Anti Infect Ther*. 2013;11(6):623–639.
9. Ho M, Webster HK, Tongtawe P, Pattanapanyasat K, Weidanz WP. Increased gamma delta T cells in acute Plasmodium falciparum malaria. *Immunol Lett*. 1990;25(1-3):139–141.
10. Behr C, Dubois P. Preferential expansion of Vγ9 Vδ2 T cells following stimulation of peripheral blood lymphocytes with extracts of Plasmodium falciparum. *Int Immunol*. 1992;4(3):361–366.
11. Elloso MM, van der Heyde HC, vande Waa JA, Manning DD, Weidanz WP. Inhibition of Plasmodium falciparum in vitro by human gamma delta T cells. *J Immunol*. 1994;153(3):1187–1194.
12. Costa G, et al. Control of Plasmodium falciparum erythrocytic cycle: γδ T cells target the red blood cell-invasive merozoites. *Blood*. 2011;118(26):6952–6962.
13. Jagannathan P, et al. Loss and dysfunction of Vδ2$^+$ γδ T cells are associated with clinical tolerance to malaria. *Sci Transl Med*. 2014;6(251):251ra117.
14. Brodin P, et al. Variation in the human immune system is largely driven by non-heritable influences. *Cell*. 2015;160(1-2):37–47.
15. Thome JJ, et al. Early-life compartmentalization of human T cell differentiation and regulatory function in mucosal and lymphoid tissues. *Nat Med*. 2016;22(1):72–77.
16. Day CL, et al. PD-1 expression on HIV-specific T cells is associated with T-cell exhaustion and disease progression. *Nature*. 2006;443(7109):350–354.
17. Wherry EJ, et al. Molecular signature of CD8+ T cell exhaustion during chronic viral infection. *Immunity*. 2007;27(4):670–684.
18. Virgin HW, Wherry EJ, Ahmed R. Redefining chronic viral infection. *Cell*. 2009;138(1):30–50.
19. Moormann AM, et al. Exposure to holoendemic malaria results in elevated Epstein-Barr virus loads in children. *J Infect Dis*. 2005;191(8):1233–1238.
20. Odiere MR, et al. Geographical distribution of schistosomiasis and soil-transmitted helminths among school children in informal settlements in Kisumu City, Western Kenya. *Parasitology*. 2011;138(12):1569–1577.

21. Won KY, et al. Assessment of quality of life as a tool for measuring morbidity due to Schistosoma mansoni infection and the impact of treatment. *Am J Trop Med Hyg*. 2014;90(2):322–328.
22. Ishizuka IE, et al. Single-cell analysis defines the divergence between the innate lymphoid cell lineage and lymphoid tissue-inducer cell lineage. *Nat Immunol*. 2016;17(3):269–276.
23. Björklund ÅK, et al. The heterogeneity of human CD127(+) innate lymphoid cells revealed by single-cell RNA sequencing. *Nat Immunol*. 2016;17(4):451–460.
24. Dadi S, et al. Cancer Immunosurveillance by Tissue-Resident Innate Lymphoid Cells and Innate-like T Cells. *Cell*. 2016;164(3):365–377.
25. Piriou E, et al. Early age at time of primary Epstein-Barr virus infection results in poorly controlled viral infection in infants from Western Kenya: clues to the etiology of endemic Burkitt lymphoma. *J Infect Dis*. 2012;205(6):906–913.
26. Reynaldi A, et al. Impact of Plasmodium falciparum Coinfection on Longitudinal Epstein-Barr Virus Kinetics in Kenyan Children. *J Infect Dis*. 2016;213(6):985–991.
27. Shekhar K, Brodin P, Davis MM, Chakraborty AK. Automatic Classification of Cellular Expression by Nonlinear Stochastic Embedding (ACCENSE). *Proc Natl Acad Sci USA*. 2014;111(1):202–207.
28. Levine JH, et al. Data-Driven Phenotypic Dissection of AML Reveals Progenitor-like Cells that Correlate with Prognosis. *Cell*. 2015;162(1):184–197.
29. Jamieson AR, Giger ML, Drukker K, Li H, Yuan Y, Bhooshan N. Exploring nonlinear feature space dimension reduction and data representation in breast Cadx with Laplacian eigenmaps and t-SNE. *Med Phys*. 2010;37(1):339–351.
30. Amir el-AD, et al. viSNE enables visualization of high dimensional single-cell data and reveals phenotypic heterogeneity of leukemia. *Nat Biotechnol*. 2013;31(6):545–552.
31. Trautmann A, et al. Human CD8 T cells of the peripheral blood contain a low CD8 expressing cytotoxic/effector subpopulation. *Immunology*. 2003;108(3):305–312.
32. Kienzle N, Baz A, Kelso A. Profiling the CD8low phenotype, an alternative career choice for CD8 T cells during primary differentiation. *Immunol Cell Biol*. 2004;82(1):75–83.
33. Xiao Z, Mescher MF, Jameson SC. Detuning CD8 T cells: down-regulation of CD8 expression, tetramer binding, and response during CTL activation. *J Exp Med*. 2007;204(11):2667–2677.
34. Zheng J, et al. Efficient induction and expansion of human alloantigen-specific CD8 regulatory T cells from naive precursors by CD40-activated B cells. *J Immunol*. 2009;183(6):3742–3750.
35. Harland KL, et al. Epigenetic plasticity of Cd8a locus during CD8(+) T-cell development and effector differentiation and reprogramming. *Nat Commun*. 2014;5:3547.
36. Møller HJ, de Fost M, Aerts H, Hollak C, Moestrup SK. Plasma level of the macrophage-derived soluble CD163 is increased and positively correlates with severity in Gaucher's disease. *Eur J Haematol*. 2004;72(2):135–139.
37. Schaer DJ, et al. Soluble hemoglobin-haptoglobin scavenger receptor CD163 as a lineage-specific marker in the reactive hemophagocytic syndrome. *Eur J Haematol*. 2005;74(1):6–10.
38. Weaver LK, et al. Pivotal advance: activation of cell surface Toll-like receptors causes shedding of the hemoglobin scavenger receptor CD163. *J Leukoc Biol*. 2006;80(1):26–35.
39. Kazankov K, et al. Soluble CD163, a macrophage activation marker, is independently associated with fibrosis in patients with chronic viral hepatitis B and C. *Hepatology*. 2014;60(2):521–530.
40. Chang JT, Wherry EJ, Goldrath AW. Molecular regulation of effector and memory T cell differentiation. *Nat Immunol*. 2014;15(12):1104–1115.
41. Geginat J, et al. Immunity to Pathogens Taught by Specialized Human Dendritic Cell Subsets. *Front Immunol*. 2015;6:527.
42. Haque A, et al. Granzyme B expression by CD8+ T cells is required for the development of experimental cerebral malaria. *J Immunol*. 2011;186(11):6148–6156.
43. Bijker EM, et al. Cytotoxic markers associate with protection against malaria in human volunteers immunized with Plasmodium falciparum sporozoites. *J Infect Dis*. 2014;210(10):1605–1615.
44. Bijker EM, Schats R, Visser LG, Sauerwein RW, Scholzen A. Ex vivo lymphocyte phenotyping during Plasmodium falciparum sporozoite immunization in humans. *Parasite Immunol*. 2015;37(11):590–598.
45. Obiero JM, et al. Impact of malaria preexposure on antiparasite cellular and humoral immune responses after controlled human malaria infection. *Infect Immun*. 2015;83(5):2185–2196.
46. Buchholz VR, Schumacher TN, Busch DH. T Cell Fate at the Single-Cell Level. *Annu Rev Immunol*. 2016;34:65–92.
47. Beaumier CM, et al. CD4 downregulation by memory CD4+ T cells in vivo renders African green monkeys resistant to progressive SIVagm infection. *Nat Med*. 2009;15(8):879–885.
48. Murayama Y, et al. CD4 and CD8 expressions in African green monkey helper T lymphocytes: implication for resistance to SIV infection. *Int Immunol*. 1997;9(6):843–851.
49. Murayama Y, Mukai R, Inoue-Murayama M, Yoshikawa Y. An African green monkey lacking peripheral CD4 lymphocytes that retains helper T cell activity and coexists with SIVagm. *Clin Exp Immunol*. 1999;117(3):504–512.
50. Oliveira-Prado R, et al. CD4 and CD8 distribution profile in individuals infected by Schistosoma mansoni. *Scand J Immunol*. 2009;69(6):521–528.
51. Seiler MP, et al. Elevated and sustained expression of the transcription factors Egr1 and Egr2 controls NKT lineage differentiation in response to TCR signaling. *Nat Immunol*. 2012;13(3):264–271.
52. Carlson CM, et al. Kruppel-like factor 2 regulates thymocyte and T-cell migration. *Nature*. 2006;442(7100):299–302.
53. Weinreich MA, Takada K, Skon C, Reiner SL, Jameson SC, Hogquist KA. KLF2 transcription-factor deficiency in T cells results in unrestrained cytokine production and upregulation of bystander chemokine receptors. *Immunity*. 2009;31(1):122–130.
54. Chaix J, et al. Cutting edge: CXCR4 is critical for CD8+ memory T cell homeostatic self-renewal but not rechallenge self-renewal. *J Immunol*. 2014;193(3):1013–1016.
55. Rothenberg EV. Transcriptional control of early T and B cell developmental choices. *Annu Rev Immunol*. 2014;32:283–321.
56. Bergsbaken T, Bevan MJ. Proinflammatory microenvironments within the intestine regulate the differentiation of tissue-resident CD8$^+$ T cells responding to infection. *Nat Immunol*. 2015;16(4):406–414.

57. Pollizzi KN, et al. Asymmetric inheritance of mTORC1 kinase activity during division dictates CD8(+) T cell differentiation. *Nat Immunol*. 2016;17(6):704–711.
58. Verbist KC, et al. Metabolic maintenance of cell asymmetry following division in activated T lymphocytes. *Nature*. 2016;532(7599):389–393.
59. Long EO, Kim HS, Liu D, Peterson ME, Rajagopalan S. Controlling natural killer cell responses: integration of signals for activation and inhibition. *Annu Rev Immunol*. 2013;31:227–258.
60. Joshi NS, et al. Inflammation directs memory precursor and short-lived effector CD8(+) T cell fates via the graded expression of T-bet transcription factor. *Immunity*. 2007;27(2):281–295.
61. Kumari S, et al. Leishmania donovani skews the CD56(+) Natural Killer T cell response during human visceral leishmaniasis. *Cytokine*. 2015;73(1):53–60.
62. Lai YS, et al. Spatial distribution of schistosomiasis and treatment needs in sub-Saharan Africa: a systematic review and geostatistical analysis. *Lancet Infect Dis*. 2015;15(8):927–940.
63. Lugli E, et al. Identification, isolation and in vitro expansion of human and nonhuman primate T stem cell memory cells. *Nat Protoc*. 2013;8(1):33–42.
64. FastQC: A Quality Control tool for High Throughput Sequence Data. Babraham Institute. http://www.bioinformatics.babraham.ac.uk/projects/fastqc/. Accessed June 28, 2017.
65. FASTX-Toolkit. Hannon Lab. http://hannonlab.cshl.edu/fastx_toolkit/. Accessed June 28, 2017.
66. Li B, Dewey CN. RSEM: accurate transcript quantification from RNA-Seq data with or without a reference genome. *BMC Bioinformatics*. 2011;12:323.
67. Love MI, Huber W, Anders S. Moderated estimation of fold change and dispersion for RNA-seq data with DESeq2. *Genome Biol*. 2014;15(12):550.
68. Mootha VK et al. Reply to "Statistical concerns about the GSEA procedure". Nat. *Genet*. 2004;36(7):663.